www.nature.com/aps

Acta Pharmacologica Sinica

ARTICLE

Tetramethylpyrazine prevents liver fibrotic injury in mice by targeting hepatocyte-derived and mitochondrial DNA-enriched extracellular vesicles

Ya-jing Li[1], Run-ping Liu[2], Ming-ning Ding[1], Qi Zheng[2], Jian-zhi Wu[1], Xiao-yong Xue[1], Yi-qing Gu[2], Bo-ning Ma[1], Ya-jie Cai[2], Shuo Li[2], Sheng Lin[3], Lu-yong Zhang[4] and Xiaojiaoyang Li[1]

Liver fibrosis is the common consequence of almost all liver diseases and has become an urgent clinical problem without efficient therapies. Recent evidence has shown that hepatocytes-derived extracellular vesicles (EVs) play important roles in liver pathophysiology, but little is known about the role of damaged hepatocytes-derived EVs in hepatic stellate cell (HSC) activation and following fibrosis. Tetramethylpyrazine (TMP) from *Ligusticum wallichii Franchat* exhibits a broad spectrum of biological activities including liver protection. In this study, we investigated whether TMP exerted liver-protective action through regulating EV-dependent intercellular communication between hepatocytes and HSCs. Chronic liver injury was induced in mice by CCl_4 (1.6 mg/kg, i.g.) twice a week for 8 weeks. In the last 4 weeks of CCl_4 administration, mice were given TMP (40, 80, 160 $mg{\cdot}kg^{-1}{\cdot}d^{-1}$, i.g.). Acute liver injury was induced in mice by injection of a single dose of CCl_4 (0.8 mg/kg, i.p.). After injection, mice were treated with TMP (80 mg/kg) every 24 h. We showed that TMP treatment dramatically ameliorated CCl_4-induced oxidative stress and hepatic inflammation as well as acute or chronic liver fibrosis. In cultured mouse primary hepatocytes (MPHs), treatment with CCl_4 or acetaminophen resulted in mitochondrial dysfunction, release of mitochondrial DNA (mtDNA) from injured hepatocytes to adjacent hepatocytes and HSCs through EVs, mediating hepatocyte damage and fibrogenic responses in activated HSCs; pretreatment of MPHs with TMP (25 μM) prevented all these pathological effects. Transplanted serum EVs from TMP-treated mice prevented both initiation and progression of liver fibrosis caused by CCl_4. Taken together, this study unravels the complex mechanisms underlying the protective effects of TMP against mtDNA-containing EV-mediated hepatocyte injury and HSC activation during liver injury, and provides critical evidence inspiring the development of TMP-based innovative therapeutic agents for the treatment of liver fibrosis.

Keywords: liver fibrosis; tetramethylpyrazine; CCl_4; acetaminophen; extracellular vesicle; intercellular communication; mouse primary hepatocytes; hepatic stellate cells

Acta Pharmacologica Sinica (2022) 43:2026–2041; https://doi.org/10.1038/s41401-021-00843-w

INTRODUCTION

Liver fibrosis is a common conjoint consequence of almost all chronic hepatopathies and is characterized by the net deposition of extracellular matrix (ECM) derived from activated hepatic stellate cells (HSCs). If left untreated, persistent liver abnormalities will further progress to end-stage cirrhosis or hepatocellular carcinoma [1]. Liver fibrogenesis is a multi-cellular response regardless of etiologies. Hepatocytes represent primary "responding" cells, which are predisposed to various damages like toxic chemicals, alcohol abuse, oxidative stress, and chronic viral infection. From a mechanistic perspective, injured hepatocytes that undergo devastating processes like apoptosis, necrosis, ferroptosis, and pyroptosis further reconstruct the microenvironment by releasing various intracellular signals, including but not limited to extracellular vesicles (EVs), damage-associated molecular patterns (DAMPs), sphingolipids, cytokines, and chemokines. These signals may regulate the survival of hepatocytes and result in the recruitment of other immune cells into the injury site, which promotes the transdifferentiation of quiescent HSCs (qHSCs) into myofibroblast-like activated HSCs (aHSCs) and subsequently trigger pro-fibrogenic reactions. However, which specific signals contribute to the intercellular crosstalk between hepatocytes and HSCs and whether these signals are pharmacologically targetable remain obscure.

EVs, known as nanometer-sized and membrane-bound vesicles, are formed by budding from plasma membranes, released into the extracellular milieu and absorbed by membrane fusion or endocytosis under physiological and pathological circumstances [2]. Due to their superior stability and bioavailability, EVs function as highly efficient messengers of producer cells, which transfer DNA fragments, DAMPs, long non-coding RNAs (lncRNAs), microRNAs (miRNAs), mRNAs, and proteins to recipient cells in a

[1]School of Life Sciences, Beijing University of Chinese Medicine, Beijing 100029, China; [2]School of Chinese Materia Medica, Beijing University of Chinese Medicine, Beijing 100029, China; [3]Key Laboratory of Chinese Internal Medicine of Ministry of Education and Beijing, Dongzhimen Hospital, Beijing University of Chinese Medicine, Beijing 100029, China and [4]Center for Drug Screening and Pharmacodynamics Evaluation, School of Pharmacy, Guangdong Pharmaceutical University, Guangzhou 510006, China
Correspondence: Xiaojiaoyang Li (xiaojiaoyang.li@bucm.edu.cn)
These authors contributed equally: Ya-jing Li, Run-ping Liu

Received: 8 October 2021 Accepted: 10 December 2021
Published online: 13 January 2022

paracrine or autocrine manner [3]. Recent studies have emphasized the critical roles of hepatocyte-derived EVs played in several liver diseases. Ceramide, a basic sphingolipid, was reported to be strikingly increased by the transfection of ERN1 adenovirus and further enriched in hepatocyte-releasing EVs, which contributed to the recruitment of monocyte-derived macrophages to the hepatic microenvironment and liver inflammation in rats and patients with steatohepatitis [4]. EV cargo MiR-1 was enriched in steatotic hepatocyte-derived EVs and engulfed by vascular endothelial cells, leading to endothelial inflammation through the suppression of Kruppel-like factor 4 and the activation of NF-κB pathway in a fatty liver mouse model [5]. In addition to these above adopter cells, hepatocyte-released EVs also can be phagocytosed by HSCs, which subsequently mediate the early transcription of fibrosis-related genes. Furthermore, after exposure to miR-128-3p-containing EVs from lipid-laden hepatocytes, more qHSCs were differentiated to aHSCs accompanied by cell migration and proliferation [6]. A recent study specifically highlighted the pro-fibrogenic role of mitochondria-derived DAMPs from hepatocytes played in HSC activation and fibrogenesis [7]. Unlike released from damaged hepatocytes, EVs derived from normal hepatocytes with different biological properties were also efficiently bound to HSCs in vivo [8] and protected from carbon tetrachloride (CCl_4)-induced fibrosis by targeting α-smooth muscle actin (α-SMA) post-transcriptional regulation [9]. However, specific cargo in these EVs was not clarified. Hence, hepatocyte-derived EVs may either trigger or delay fibrogenesis depending on the composition of cargo and the different pathological statuses of both producer cells and recipient cells. Most recently, as a newly identified cargo, mitochondrial DNA (mtDNA) was also found to be enriched in EVs derived from virus-infected hepatocytes [10]. However, the effects of mtDNA in hepatocytes-derived EVs on hepatocyte damage or HSC activation are not well characterized and whether the EVs-mediated intercellular communication in fibrosis, if exists, can be alleviated by any pharmacological therapies is unknown.

Emerging evidence suggests that pharmacological approaches targeting vital cell-to-cell communication among liver cells may influence the progression of liver fibrosis. However, in addition to the very long process of drug development and enormous investments made by pharmacological industries, most of the current therapies against acute or chronic liver fibrosis are usually focused on a single target, and their anti-fibrotic effects in clinical trials are limited and inconsistent. Bioactive ingredients derived from natural medicines are generally considered to be safe and have been clinically used for thousands of years, representing promising therapeutic strategies for liver fibrosis. Tetramethylpyrazine/ligustrazine (TMP, PubChem CID: 14296) is the main characteristic alkaloid isolated from *Ligusticum wallichii Franchat* and exerts a broad spectrum of biological activities, including anti-cancer, anti-atherogenesis, anti-angiogenesis and anti-inflammation [11, 12]. Recently, TMP was reported to exert therapeutic promise for liver fibrosis via preventing HSC activation and improving vascular remodeling [13]. However, how TMP implicates the intercellular communication between liver cells during fibrogenesis remains elusive. Based on the above studies and existing questions, there is an unmet need for investigating whether and how TMP regulates the intercellular communication between different cells in the hepatic microenvironment, especially for hepatocytes and HSCs.

In pursuing our hypothesis, we explored the hepatoprotective effects of TMP on acute or chronic fibrotic liver injury using different mouse models along with in vitro complementary approaches. Our data supported that TMP suppressed hepatic oxidative stress, increased mitochondrial membrane potential, prevented the release of hepatocyte-derived and mtDNA-containing EVs, and subsequently inhibited the mtDNA-induced adjacent hepatocyte damage and HSC activation. Transplant of serum EVs from TMP-treated mice not only alleviated the onset but also the progression of CCl_4-induced liver fibrosis in vivo, in association with decreased circulating mtDNA, reduced hepatic oxidative stress and attenuated fibrogenesis. Our results highlight the significance of mtDNA-containing EVs-mediated intercellular communication between hepatocytes and HSCs and further provide novel insights into the anti-fibrotic mechanism of TMP.

MATERIALS AND METHODS

Materials

CCl_4 (A33986) and TMP (A45751) were purchased from Innochem (Beijing, China). Acetaminophen (APAP) (S31044) was obtained from Yuanye Bio-Technology (Shanghai, China). Collagen type I from rat tail (C3867), Williams' Medium E with *L*-glutamine (W4125), collagenase from *Clostridium histolyticum* (C5138), and other cell culture supplemental reagents were all obtained from Sigma (St. Louis, USA). The antibody against anti-DNA (CBL186) was obtained from Merck Millipore (Darmstadt, Germany). The antibody against CD63 (ab216130) was purchased from Abcam (Cambridge, USA). Antibodies against TOM20 (11802-1-AP), FIBRONECTIN (15613-1-AP) and ALB (16475-1-AP) were purchased from Proteintech Group (Rosemont, USA). The antibody against CD81 (10037S) was obtained from Cell Signaling Technology (Danvers, USA). Goat anti-mouse IgG (H+L) Highly Cross-Adsorbed secondary antibody (Alexa Fluor Plus 488) (Ul287767) was purchased from Thermo Fisher Scientific (Waltham, USA) and goat anti-rabbit IgG (H+L), F(ab')2 Fragment (Alexa Fluor 594 Conjugate) (8889S) was purchased from Cell Signaling Technology (Danvers, USA).

Animal study

C57BL/6J mice (7-week-old, male and female) were purchased from Vital River Laboratory Animal Technology (Beijing, China) and were kept under 12 h light–dark cycle at a consistent temperature (22 ± 2 °C) and provided with standard chow with access to sterile water *ad libitum*. For CCl_4 chronic injury experiments (Fig. 1), mice were divided into five groups ($n = 6$): (1) control group; (2) CCl_4 group; (3) CCl_4 + TMP (low dose, 40 mg/kg) group; (4) CCl_4 + TMP (medium dose, 80 mg/kg) group; (5) CCl_4 + TMP (high dose, 160 mg/kg) group. Groups (2)–(5) were orally administered CCl_4 at a dose of 1.6 mg/kg twice a week for 8 weeks. In the last 4 weeks of CCl_4 administration, groups (3)–(5) were treated with different dosages of TMP once daily by gavage. At the end of treatment, mice were sacrificed. For CCl_4 acute injury experiments (Fig. 6), mice were divided into seven groups ($n = 6$): (1) control group; (2) CCl_4 24 h group; (3) CCl_4 + TMP 24 h group; (4) CCl_4 48 h group; (5) CCl_4 + TMP 48 h group; (6) CCl_4 96 h group; (7) CCl_4 + TMP 96 h group. Groups (2)–(7) were all intraperitoneally injected with a single dose of CCl_4 (0.8 mg/kg). One hour after the injection of CCl_4, groups (3), (5), and (7) were orally treated with TMP (80 mg/kg) every 24 h. Mice in groups (2) and (3), (4) and (5), and (1), (6), and (7) were sacrificed at 24, 48, and 96 h, respectively. In addition, serum EVs from mice in groups (1), (4), and (5) were isolated and referred to as SEV-Ct, SEV-CCl_4, and SEV-CCl_4 + TMP for further EVs tail vein injection experiments (Figs. 7 and 8). In the acute experiment of EVs tail vein injection (Fig. 7), mice were divided into three groups ($n = 6$): (1) SEV-Ct group; (2) SEV-CCl_4 group; (3) SEV-CCl_4 + TMP group. Groups (1)–(3) were administered different serum EVs ($4 \times e^8$ particles per mouse) via tail vein injection for one time. Mice were sacrificed 48 h later. For the chronic experiment of EVs tail vein injection (Fig. 8), mice were treated with CCl_4 or olive oil once a week for 3 weeks and then administrated with SEV-Ct, SEV-CCl_4 and SEV-CCl_4 + TMP by tail vein injection at day 3 and day 5 post last CCl_4 injection ($n = 6$). Mice were anesthetized with isoflurane and sacrificed at the end of the fourth week. After being sacrificed at corresponding times, mouse serum was collected and liver samples were harvested and stored in a −80 °C freezer. All animal studies and procedures were performed in accordance with the guidelines of the Institutional

Animal Care and Use Committee of Beijing University of Chinese Medicine.

RNA-sequencing analysis

Total RNA was extracted from mouse livers and quantitated by NanoRhatometer® spectrophotometer (IMPLEN, USA). RNA integrity was measured using the RNA Nano Assay kit. mRNA was purified from total RNA by poly-T oligo-attached magnetic beads. After cDNA synthesis, the library fragments were purified with the AMPure XP system (Beckman Coulter, USA) to enrich 250–300 bp cDNA fragments. NEBNext Ultra™ RNA Library Prep Kit for Illumina (NEB) was used to establish a sequencing library. The sequencing library was further generated on an Illumina Novaseq platform, as previously described [14]. Gene expression data normalization and differential gene expression were performed using the edgeR R package. Gene Ontology (GO) enrichment analysis of differentially expressed genes (DEGs) was performed using the cluster Profiler R package. Based on the GO dataset, differential expression data were further analyzed by Gene Set Enrichment Analysis. The heatmaps and hierarchical cluster analysis were performed to visualize distinguishable regulated mRNAs.

Isolation and culture of mouse primary hepatocyte (MPH) and HSC

MPHs were isolated by a two-step collagenase perfusion method and cultured with Williams' Medium E supplemented with dexamethasone (0.1%) and *L*-thyroxine (0.1%). Mouse HSCs were isolated using a gradient centrifugation method and cultured with Dulbecco's Modified Eagle's Medium supplemented with 10% FBS, penicillin G (100 U/mL) and streptomycin (100 μg/mL) according to our previous report [15].

Isolation of EVs

Mouse serum was firstly centrifuged for 15 min at 1200 g to remove debris, followed by ultracentrifugation at 100,000 g for 90 min. For isolation of EVs from conditional medium, after pretreated with 25 μM TMP for 1 h, MPHs plated on 100-mm dishes were treated with 10 mM CCl_4 and 8 mM APAP for 24 h. Following the 500 g centrifugation for 10 min, the cleared supernatant without cell debris was transferred to new Eppendorf tubes and centrifuged for 10 min at 2000 g. Finally, MPH-derived EVs in the supernatant were isolated by ultracentrifugation at 100,000 g for 60 min. The EV pellets were then washed and re-suspend in sterile phosphate buffer saline (PBS) and stored at −80 °C for further experiments. All above ultracentrifugation was performed at 4 °C using Sorvall WX 100+ ultracentrifuge from Thermo Fisher Scientific (Waltham, USA).

Isolation and characterization of mitochondrial DNA

Total DNA was isolated and purified from EVs in mouse serum and cell culture medium by Gentra Puregene Cell Kit (158745, QIAGEN) following the manufacturer's instruction. mtDNA was quantified by qPCR and then identified using DNA gel electrophoresis.

EVs uptake assay

MPHs were treated as indicated and collected conditional medium for EV isolation. After ultracentrifugation and purification, EVs were first labeled with the PKH26 dye and then incubated with HSCs for 3 h. At the end of treatment, HSCs were completely rinsed, fixed by 4% paraformaldehyde (PFA) and stained with DAPI. All images were captured by Olympus FV3000 confocal laser scanning microscopy (Tokyo, Japan).

Immunofluorescence staining

For ALB immunofluorescence staining, MPHs were washed 3 times with PBS and fixed with PFA for 30 min, followed by blocking in 1% PBS–bovine serum albumin supplemented with 0.1% Trion-X-100. MPHs were then incubated with primary antibody against ALB and washed with PBS, followed by staining with an anti-rabbit secondary Alexa Fluor (594) antibody. For co-immunofluorescence staining experiments, cells were fixed, permeabilizated and blocked as above described. Then cells were concurrently incubated with primary antibodies against TOM20 and DNA, and stained with anti-mouse secondary Alexa Fluor (488) and anti-rabbit secondary Alexa Fluor (594) antibodies. All cells were counterstained using DAPI and imaged by Olympus FV3000 confocal laser scanning microscopy (Tokyo, Japan).

Reactive oxygen species (ROS) and mito-tracker molecular probes

ROS assay kit (S0033) and mito-tracker red CMXROS kit (C1049) obtained from Beyotime Biotechnology (Shanghai, China) were used for the detection of mitochondria and cellular production of ROS. After 24 h treatment, MPHs were stained with 10 μM DCFH-DA and 100 nM CMXROS for 20 min. After washing and staining with DAPI, MPHs were imaged by Olympus FV3000 confocal laser scanning microscopy (Tokyo, Japan).

Statistical analysis

All results were repeated at least three independent times and were expressed as mean ± SEM. Comparison of data was performed using a one-way ANOVA and Tukey's post hoc test between multiple groups in GraphPad Prism Software 8.0 (GraphPad, San Diego, CA, USA). A P value of ≤0.05 was considered statistically significant.

Please see the Supporting Information for a detailed description of other experimental materials and methods.

RESULTS

TMP ameliorates CCl_4-induced chronic liver fibrosis in mice

To examine the protective effects of TMP on chronic liver fibrosis, mice were first administered CCl_4 (1.6 mg/kg) for 4 weeks, followed by TMP treatment (40, 80, and 160 mg/kg) for an additional 4 weeks along with continuous CCl_4 challenges (Fig. 1a). CCl_4 markedly induced liver injury, as indicated by increased serum levels of aspartate aminotransferase (AST) and alanine aminotransferase (ALT), which were markedly reduced by TMP treatment (Fig. 1b). As shown in Fig. 1c, TMP significantly reversed CCl_4-caused ballooning changes of hepatocytes, lobular inflammation, and collagen deposition as illustrated by hematoxylin & eosin (H&E) and Masson's trichrome staining. Immunohistochemistry staining of fibronectin, a specific marker of liver fibrosis, indicated that TMP treatment dramatically decreased CCl_4-induced fibronectin. To systematically investigate the underlying mechanisms and potential targets of TMP against chronic liver fibrosis, RNA-sequencing analysis was performed to determine the DEGs between CCl_4 group and CCl_4 + TMP group. As shown in Supplementary Fig. S1a, a total of 501 genes were identified as DEGs ($P < 0.05$) in the CCl_4 group compared with the control group (365 upregulated DEGs and 136 downregulated DEGs). The physiological degradation of ECM and re-epithelialization were crucial features of tissue repair and remodeling. DEGs implicated in ECM balance were plotted in Fig. 1d as a heatmap. DEGs identified in both CCl_4 *vs* Ct and CCl_4 + TMP vs CCl_4 groups were further categorized into three clusters by hierarchical cluster analysis (Fig. 1d). The expression of DEGs in cluster 1 was downregulated in the CCl_4 group, which was further decreased after TMP treatment. The expression of DEGs in cluster 2, several critical genes involved in collagen degradation including matrix metalloproteinase 14 (*Mmp14*), a disintegrin and metalloproteinase with thrombospondin motifs 7 (*Adamts7*), *Adamts12* and *Adam15* was remarkably upregulated in CCl_4 + TMP group when compared to CCl_4 group. The CCl_4-induced upregulation of collagen synthetic-related genes in cluster 3, such as lysyl oxidase homolog 2 (*Loxl2*), collagen type IV alpha 1 chain (*Col4a1*), *Col12a1* and *Ecm2*, were significantly downregulated by TMP. As shown in Fig. 1e, qPCR results demonstrated that TMP significantly

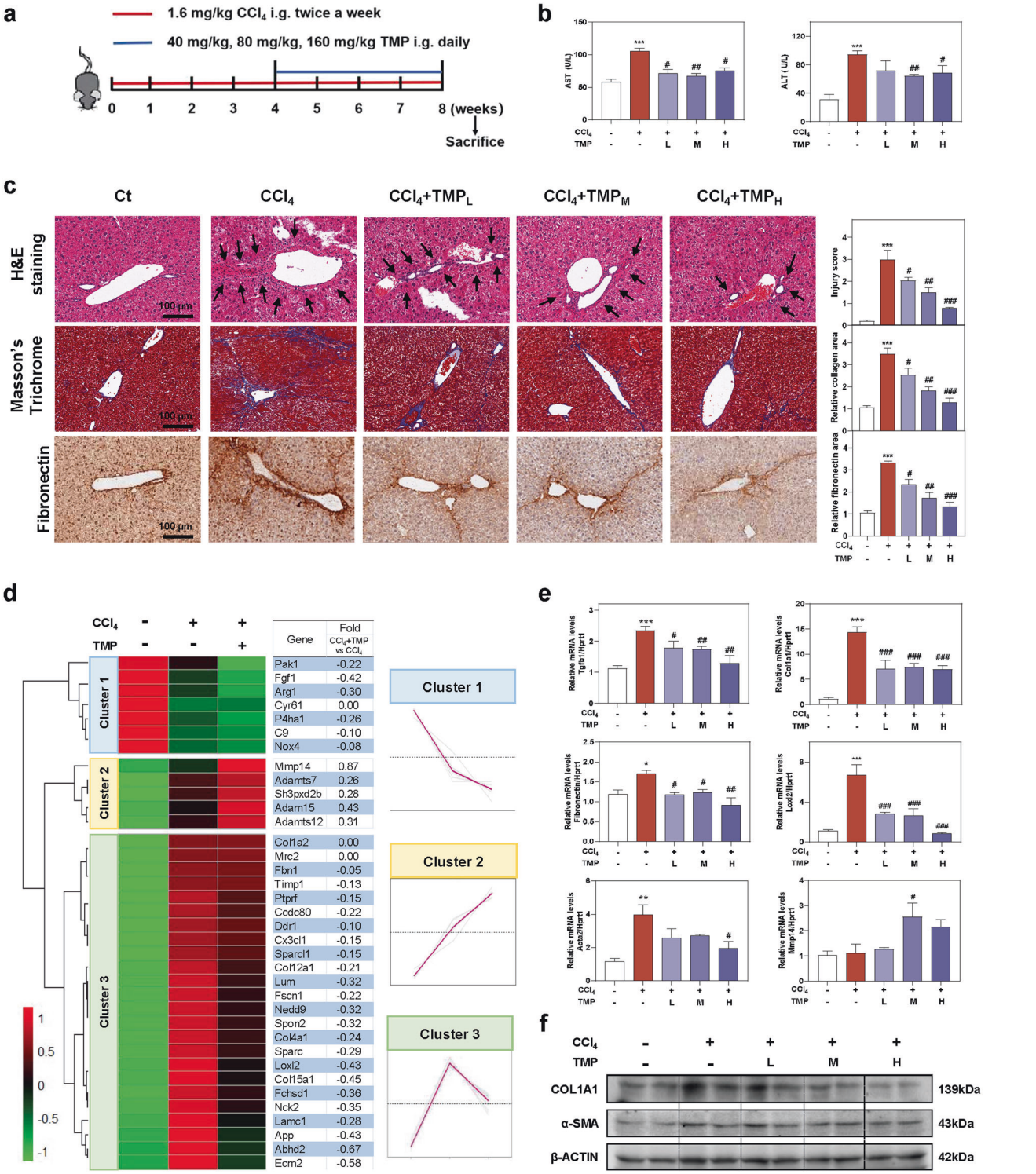

Fig. 1 TMP ameliorates CCl_4-induced hepatic fibrosis and liver injury. Mice were administered CCl_4 (1.6 mg/kg) and different dosages (40, 80, and 160 mg/kg) of TMP by gavage. **a** Experimental protocol. **b** AST and ALT levels in serum. **c** Representative images of H&E, Masson's Trichrome, and fibronectin staining. The immunostaining was quantified by Image J software. Scale bar = 100 μm. **d** The relative expression levels of DEGs enriched in ECM synthesis and degradation pathways were shown as a heatmap. Average log2 fold changes of CCl_4 + TMP vs CCl_4 groups were presented in the right panel. The expression of DEGs was classified into three clusters and the trend lines presenting the hepatic changes of these DEGs were shown. **e** Relative mRNA levels of *Tgfb1*, *Col1a1*, *Fibronectin*, *Loxl2*, *Acta2*, and *Mmp14* were determined by qPCR and normalized using *Hprt1* as an internal control. **f** Representative immunoblots against COL1A1, α-SMA, and β-ACTIN were shown. Statistical significance: $^{*}P < 0.05$, $^{**}P < 0.01$, $^{***}P < 0.001$, compared with control group; $^{\#}P < 0.05$, $^{\#\#}P < 0.01$, $^{\#\#\#}P < 0.001$, compared with CCl_4 group ($n = 6$).

decreased the mRNA expression of transforming growth factor beta-1 (*Tgfb1*), collagen type I alpha I chain (*Col1a1*), *fibronectin* and *Loxl2* stimulated by CCl_4. CCl_4-induced upregulation of α-smooth muscle actin (*Acta2*) was significantly reversed by TMP at a high dose. Furthermore, TMP at medium dose significantly increased the hepatic mRNA level of *Mmp14* compared to CCl_4 administration. Consistently, TMP dose-dependently decreased the protein levels of COL1A1 and α-SMA induced by CCl_4 (Fig. 1f and Supplementary Fig. S1b).

TMP alleviates CCl_4-induced oxidative stress and hepatic inflammation

Oxidative stress and inflammatory response are major causes of hepatocyte damage and function as key drivers for liver fibrogenesis. Based on the obvious anti-fibrosis effects of TMP in vivo (Fig. 1), we next examined whether the anti-fibrotic capacity of TMP was related to the prevention of oxidative stress and hepatic inflammation. Hydroxyproline not only functions as a substrate for ECM synthesis but also reacts with hydroxyl radicals generated from the decomposition of CCl_4. As shown in Fig. 2a, TMP treatment significantly reversed CCl_4-induced hydroxyproline in livers. It has been well accepted that malondialdehyde (MDA) is increased under the condition of oxidative stress, while superoxide dismutase (SOD) and glutathione (GSH) protect hepatic cells against oxygen free radical-induced damage. As shown in Fig. 2a, CCl_4 significantly stimulated oxidative stress in mice as illustrated by increased hepatic MDA and decreased SOD content; treatment of the medium and high doses of TMP prevented these pathological changes in MPHs. Interestingly, although CCl_4 gently upregulated the levels of GSH in livers, a significant increase of GSH was noted in the presence of TMP. Next, we explored the potential mechanisms involved in the TMP-mediated dynamic balance between oxidation and reduction. As shown in Fig. 2b, DEGs related to oxidative stress were plotted as a heatmap and were further categorized in 3 clusters by hierarchical cluster analysis. The expression of DEGs in cluster 1, including glutathione S-transferase theta-1 (*Gstt1*), *Gstt3* and glutathione S-transferase Mu-2 (*Gstm2*), was downregulated in the CCl_4 group, which was reversed by TMP treatment. CCl_4-induced upregulation of DEGs in cluster 2, such as glutathione peroxidase 3 (*Gpx3*) were further enhanced by TMP. In addition, the DEGs in cluster 3 such as cytochrome P450 2A4 (*Cyp2a4*), *Cyp39a1* and *Cyp3a44* were increased by CCl_4 and was further reversed by TMP. As summarized in Fig. 2c, xenobiotic compounds directly consumed GSH or were decomposed into ROS including organic hydroperoxides, superoxide anion and hydroxyl radical by Gsts, which were subsequently conjugated with GSH for elimination [16]. Furthermore, the conjugate of GSH and electrophiles were catalyzed by Gpxs to H_2O and alcohol, while GSH was oxidized to GSSG. Consistent with RNA-sequencing results, we showed that CCl_4 decreased the gene expression of *Gstt1*, which was significantly reversed by TMP. However, only a high dose of TMP significantly increased the mRNA levels of *Gpx3* and *Gstm2* (Fig. 2c). These results suggested that TMP potentially increased oxidative stress tolerance of hepatocytes by modulating the dynamic balance of the GSH-mediated antioxidant mechanism. Emerging evidence suggests that persistent oxidative stress triggers the progression of inflammatory responses and subsequently contributes to liver fibrosis. As shown in Fig. 2d, the co-treatment of CCl_4 plus TMP decreased the mRNA levels of genes associated with inflammatory reactions, including interleukin-1 beta (*Il1b*) and tumor necrosis factor-alpha (*Tnfa*) compared to the CCl_4 group. Although no significant change of *Il6* expression was observed after CCl_4 treatment, the level of *Il6* was markedly downregulated with the presence of a high dose of TMP plus CCl_4. We recently reported that lncRNA H19-enriched exosomes promoted M1 polarization of Kupffer cells and further accelerated the progression of cholestatic liver injury in mice [17]. Interestingly, after CCl_4 treatment, H19 mRNA level was significantly increased, while TMP at high dose blocked this process. Notably, critical genes involved in chemotaxis, including c-x-c chemokine receptor type 4 (*Cxcr4*), C5a anaphylatoxin chemotactic receptor 1 (*C5ar1*) and c-x3-cmotif chemokine ligand 1 (*Cx3cl1*) were all markedly increased in the CCl_4 group, which were inhibited by TMP treatment, as illustrated by the RNA-sequencing results in Fig. 2e. These results suggested that TMP prevented liver fibrosis in a complex way.

TMP alleviates oxidative stress-mediated mitochondrial damage and hepatocyte injury

Hepatocytes are major parenchymal cells responsible for bearing the brunt of oxidative stress in livers, encouraging us to explore the hepatoprotective effects of TMP on oxidative stress induced by CCl_4 and APAP. As shown in Fig. 3a and Supplementary Fig. S2a, MPHs expressed a lower ALB level upon exposure to CCl_4 or APAP, which was markedly restored after TMP treatment. In addition, TMP also restored the decreased mRNA levels of mature-hepatocyte markers, hepatocyte nuclear factor 4-alpha (*Hnf4a*) and forkhead box protein a2 (*Foxa2*) caused by CCl_4 or APAP in MPHs (Fig. 3b). Hepatocyte undergoes death in various forms, which is also considered as an initial event in liver fibrogenesis. Taking results of Figs. 1b and 3a, b into account, we next focused on the protective effects of TMP on hepatocyte death. Flow cytometry studies in Fig. 3c confirmed that both CCl_4 and APAP significantly increased the populations of early apoptotic hepatocytes whereas TMP effectively blocked this process (from 51.23% to 31.76% compared with the CCl_4 group and from 51.78% to 31.50% compared with the APAP group, respectively), yet only slightly decreased the portion of late apoptotic cells (from 12.92% to 10.18% compared with the CCl_4 group and from 13.52% to 12.87% compared with the APAP group, respectively). Mitochondria serve an irreplaceable role in energy generation via oxidative phosphorylation and represent a central nexus of different cell death types [18]. We further explored the correlation between TMP-mediated hepatoprotective effects and mitochondrial oxidative stress. In line with our in vivo findings in Fig. 2, TMP significantly restored the CCl_4- or APAP-stimulated oxidative stress in MPH, as revealed by downregulated MDA level and upregulated SOD activity (Fig. 3d). Although both CCl_4 and APAP were able to cause oxidative stress in the liver, the cellular damage caused by these two toxic compounds was not identical due to different metabolic pathways and biological mechanisms. Briefly, CCl_4 was conjugated with GSH and subsequently helped the oxidation of GSH, while APAP was metabolized into electrophilic intermediate *N*-acetyl-*p*-benzoquinone-imines and depleted hepatic GSH. Eventually, exhausted GSH failed to detoxify ROS and further resulted in oxidative stress in hepatocytes. We next applied live cell staining analysis to detect the production of cellular ROS (green) and mitochondria (red). As shown in Fig. 3e and Supplementary Fig. S2b, the increased ROS level in or around mitochondria caused by CCl_4 or APAP was significantly decreased with the presence of TMP. Interestingly, the production of ROS in the CCl_4 group was more diffused and nebulous compared with that in the APAP group. Excessive ROS will alter morphology, membrane permeability and function of mitochondria, leading to mitochondrial pore opening and subsequent hepatocyte death [19]. As shown in Fig. 3f, our flow cytometry results suggest that both CCl_4 and APAP significantly decreased mitochondrial membrane potential, suggesting mitochondrial damage in response to oxidative stress. As expected, TMP significantly protected against the loss of mitochondrial membrane potential.

TMP suppresses the release of mtDNA from injured hepatocytes and prevents subsequent mtDNA-dependent hepatocyte injury

Mitochondria containing DNA are extremely enriched in hepatocytes. Once oxidative stress breaks out, mtDNA is regarded as a major source of released immunogenic DAMPs that triggered

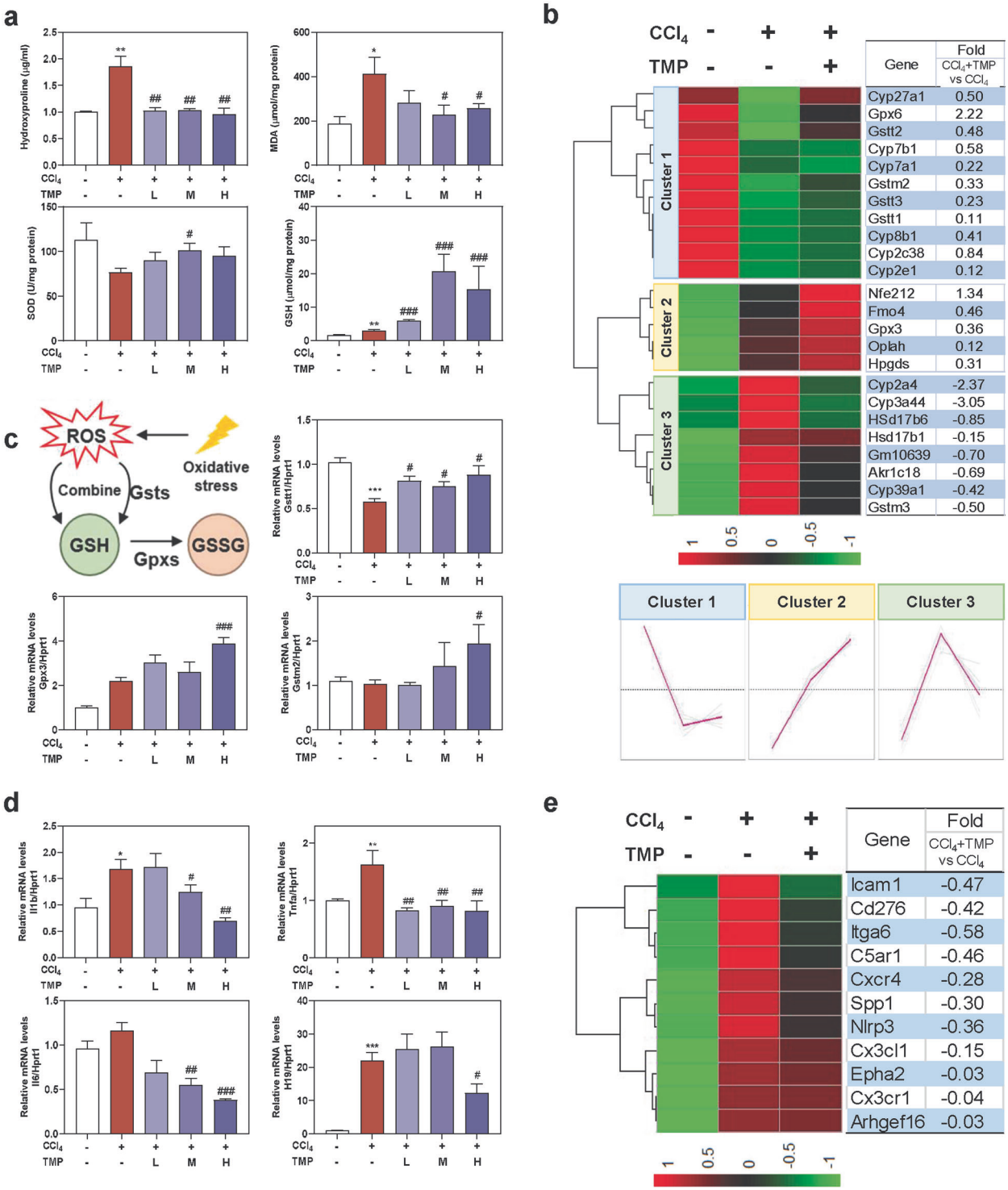

Fig. 2 TMP ameliorates CCl_4-induced oxidative stress and hepatic inflammation. Mice were treated as described in Fig. 1. **a** Liver hydroxyproline, MDA, SOD, and GSH levels in livers. **b** The relative expression levels of DEGs implicated in oxidative stress were shown as a heatmap. Average log2 fold changes of CCl_4 + TMP vs CCl_4 groups were presented in the right panel. **c** The biological process of oxidation-reduction metabolism was shown. Relative mRNA levels of **c** *Gstt1*, *Gpx3*, *Gstm2*, **d** *Il1b*, *Tnfa*, *Il6*, and *H19* were determined by qPCR and normalized using *Hprt1* as an internal control. **e** The relative expression levels of DEGs implicated in inflammatory response were shown as a heatmap. Average fold changes of CCl_4 and CCl_4 + TMP groups were presented in the right panel. Statistical significance: $^{*}P < 0.05$, $^{**}P < 0.01$, $^{***}P < 0.001$, compared with control group; $^{\#}P < 0.05$, $^{\#\#}P < 0.01$, $^{\#\#\#}P < 0.001$, compared with CCl_4 group ($n = 6$).

innate immune response and fibrogenesis [20]. We further deeply analyzed RNA-sequencing data to address whether TMP affected mitochondrial biosynthesis and the release of mtDNA in hepatocytes. As shown in Fig. 4a, CCl_4 dramatically downregulated the transcription of mitochondrial genes, including NADH-ubiquinone oxidoreductase chain 3 (*mt-Nd3*), *mt-Nd4*, *mt-Nd5*, and *mt-Nd6*, suggesting impaired biogenesis and function of mitochondria. TMP markedly upregulated the mRNA expression of

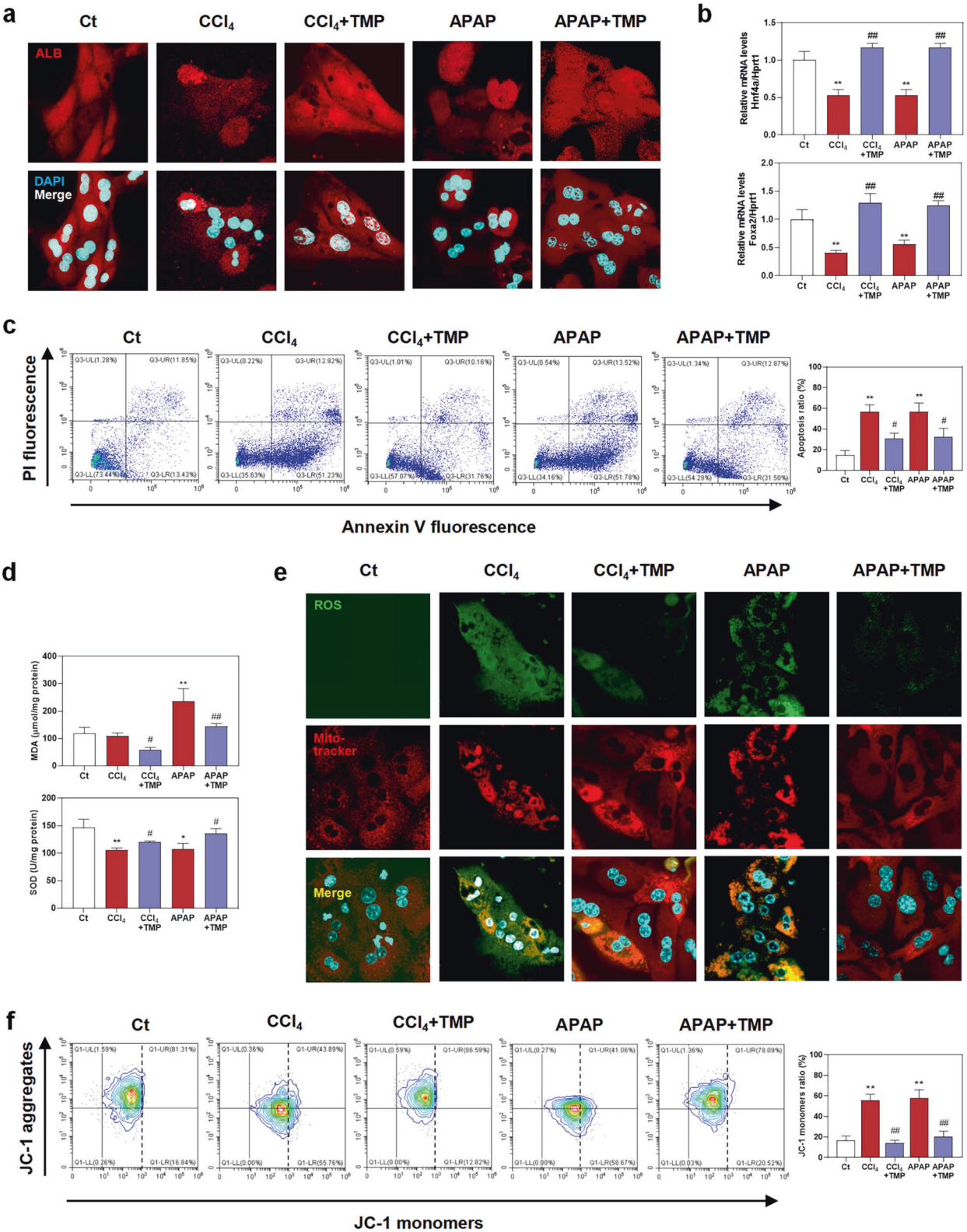

Fig. 3 TMP prevents oxidative stress, mitochondrial damage, and hepatocyte death. After pre-treated with 25 μM TMP for 1 h, MPHs were treated with 10 mM CCl_4 and 8 mM APAP for another 24 h. **a** Representative images of immunofluorescent staining of ALB. **b** Relative mRNA levels of *Hnf4a* and *Foxa2* were determined by qPCR and normalized using *Hprt1* as an internal control. **c** Flow cytometry of AV-PI with histograms. **d** MDA and SOD levels in MPHs. **e** Representative images of live cell staining of ROS and mito-tracker. **f** Flow cytometry of JC-1 with histograms. Statistical significance: $^{*}P < 0.05$, $^{**}P < 0.01$, compared with control group; $^{\#}P < 0.05$, $^{\#\#}P < 0.01$, compared with relative model group ($n = 3$).

these mtDNA-related genes by two to three folds. Furthermore, co-immunofluorescence staining of mitochondrial marker TOM20 (red dots) and anti-DNA (green dots) in Fig. 4b, c suggested that CCl_4 or APAP significantly promoted the release of mtDNA from mitochondria in MPHs (increased mtDNA outside the nucleus and mitochondria, green dots), which were significantly prevented by TMP (increased mtDNA within mitochondria, yellow dots). These results suggested that TMP not only enhanced mitochondrial biogenesis but also protected mitochondrial integrity against oxidative stress-related damages. In response to increased ROS, two proteins Bcl-2-associated X (BAX) and Bcl-2 homologous antagonist/killer (BAK) were reported to trigger the mitochondrial outer membrane permeabilization (MOMP), which contributed to the release of mitochondrial intermembrane space proteins and mtDNA and promoted cell death [21]. Given the intercellular communication among different liver cells through autocrine and paracrine manner [22], we next investigated the effects of hepatocytes-releasing mtDNA on injured hepatocytes. For this purpose, we first established a mild injured hepatocyte model induced by CCl_4 or APAP at a relatively low dose and then incubated these MPHs with EVs derived from high doses of CCl_4-, CCl_4 + TMP-, APAP- and APAP + TMP-treated MPHs (EV-CCl_4, EV-CCl_4 + TMP, EV-APAP and EV-APAP + TMP) (Fig. 4d). First, the morphology, size and purity of hepatocyte-releasing EVs isolated from the serum-free conditional medium were confirmed by TEM examination and Western blot analysis of typical EV markers (CD81 and CD63) (Fig. 4e). To investigate whether TMP decreased the release of mtDNA from mitochondria in hepatocytes, we detected the levels of representative mtDNA [23], including the 12S mtDNA region (12S), 16S and cytochrome *c* oxidase subunit I (COXI) in the cargo of hepatocyte-releasing EVs. As shown in Fig. 4f, the copy numbers of mtDNA were remarkably upregulated by CCl_4 or APAP, which were significantly downregulated by TMP. Flow cytometry results in Fig. 4g demonstrated that EV-CCl_4 and EV-APAP aggravated CCl_4- and APAP-induced mild hepatocyte death, as indicated by the higher populations of early apoptotic hepatocytes. Interestingly, EV-CCl_4 + TMP and EV-APAP + TMP did not alter the populations of early apoptotic hepatocytes caused by CCl_4 or APAP treatment alone. Moreover, pre-incubation of these EVs with DNase I depleted all mtDNA in EVs and significantly blocked EVs-induced damage. These findings suggested that damaged mitochondria-derived EVs loaded with mtDNA significantly aggravated hepatocyte death, which was completely blocked by TMP interference.

TMP hampers hepatocyte-EVs-mediated mtDNA transfer and following HSC activation

To directly assess whether the anti-fibrotic function of TMP was related to the decreased transfer of mtDNA from hepatocytes to HSCs, EV-CCl_4, EV-CCl_4 + TMP, EV-APAP, and EV-APAP + TMP isolated from the conditional medium of MPHs were used to incubate with freshly isolated mouse primary HSCs (Fig. 5a). PKH26 (a dye for phospholipid bilayer) was used to monitor the uptake of hepatocyte-releasing EVs by mouse primary HSCs. As displayed in Fig. 5b, the uptake of PKH26-labeled MPH-derived EVs by HSCs was rapid. Furthermore, our results revealed that EV-CCl_4 and EV-APAP from hepatocytes significantly increased DNA load outside nuclear and mitochondria area (shown as green dots) in HSCs, suggesting the delivery of DNA products from hepatocytes into HSCs via EVs (Fig. 5c, d). Notably, in line with the reduced release of mtDNA after TMP treatment in hepatocytes (Fig. 4), EV-CCl_4 + TMP- and EV-APAP + TMP-mediated exogenous mitochondria- and nuclear-free DNA accumulation in HSCs was significantly decreased when compared to EV-CCl_4 and EV-APAP groups (Fig. 5c, d). After 48 h of incubation with EVs derived from CCl_4- or APAP-treated MPHs, the mRNA levels of fibrotic genes, such as *Acta2*, *Col1a1*, *Fibronectin* and tissue inhibitors of metalloproteinases (*Timp1*), were significantly upregulated (Fig. 5e and Supplementary Fig. S3a). Concurrently, both EVs derived from MPHs treated with TMP in combination with toxic drugs and EV-CCl_4 or EV-APAP pre-incubated with DNase I did not affect the expression of fibrotic marker genes (Fig. 5e). Taken together, these results suggested that hepatocyte-derived and mtDNA-containing EVs played a critical role in liver fibrogenesis, while TMP inhibited mtDNA release from injured hepatocytes and thus attenuated HSC activation.

TMP reduces mtDNA loading in serum EVs and alleviates CCl_4-induced acute hepatic injury

Given the inhibitory effects of TMP on mtDNA release in hepatocytes, we hypothesized that TMP might protect injured hepatocytes against oxidative stress and decrease mtDNA loading in hepatocyte-derived circulating EVs in vivo. To test this, we established a mouse model to investigate the protective effects of TMP on the acute and recovery phase of single-dose CCl_4-induced liver injury (Fig. 6a). As shown in Fig. 6b, CCl_4 rapidly induced acute liver injury peaking at 24 h, lasting up to 48 h and disappearing at 96 h. Interestingly, both AST and ALT levels were lower in CCl_4 + TMP 24 h group compared with CCl_4 group. Biochemical quantification of hepatic oxidative stress in TMP-treated mice showed decreased MDA and increased SOD levels after 24 and 48 h CCl_4 administration. Notably, the hepatic GSH levels were compensatorily upregulated at 24 h and then dramatically exhausted 48 h after CCl_4 challenge. Although TMP had no obvious effect on GSH levels at 24 and 48 h time points compared to relative CCl_4 groups, it significantly promoted GSH recovery at 96 h after CCl_4 administration, suggesting better oxidative stress tolerance (Fig. 6c). Histological examination showed that hepatocyte necrosis and inflammation rapidly appeared after 24 h and seriously deteriorated after 48 h of CCl_4 administration. As expected, TMP significantly alleviated hepatocyte vacuolar damage and decreased inflammatory cell infiltration at almost all time points (Fig. 6d). As shown in Fig. 6e, CCl_4-induced acute injury was accompanied by a robust upregulation of pro-fibrogenic genes, including *Acta2* at 48 h, *Col1a1* and *Loxl2* at 48 and 96 h and *Timp1* at all time points, which were all inhibited by TMP treatment. Furthermore, TMP significantly increased *Mmp14* mRNA level at 96 h compared to that in the CCl_4 group (Supplementary Fig. S4a). Surprisingly, the mRNA levels of *Gstt1*, *Gstm2*, *Gpx3*, and *Gstt2*, genes involved in GSH oxidation and consumption, were decreased by CCl_4 at 24 and 48 h, but significantly increased by CCl_4 at 96 h. Interestingly, TMP markedly enhanced the increase of *Gstt1*, *Gstt2* and *Gstm2* expression at 96 h, suggesting enhanced recovery of antioxidant mechanisms (Fig. 6f and Supplementary Fig. S4b).

To further investigate whether hepatocyte-derived mtDNA was released into circulation, we isolated EVs from the serum of CCl_4- and CCl_4 + TMP-treated mice and detected the numbers and characteristics of EVs by NTA technique (Fig. 6g). The dosage of EV treatment was $3.9 \times e^9$ particles/mL. Next, we detected the amount of mtDNA by qPCR assay and confirmed the presence of mtDNA in mouse serum (Supplementary Fig. S4c). As shown in Fig. 6h and Supplementary Fig. S4d, serum mtDNA level was markedly increased in CCl_4-treated mice and was significantly decreased by TMP administration. Collectively, these findings suggested that the protective effect of TMP against CCl_4-induced liver injury might attribute to the inhibition of mtDNA release from hepatocytes.

TMP downregulates CCl_4-induced mtDNA loading in serum EVs and protects against EVs-triggered hepatic injury

To specifically elucidate the role of mtDNA-containing serum EVs in the initiation of hepatic injury, mice were injected via tail vein with (1) serum EVs derived from control mice (SEV-Ct); (2) serum EVs derived from CCl_4-treated mice (SEV-CCl_4); (3) serum EVs derived from CCl_4 + TMP-treated mice (SEV-CCl_4 + TMP) (Fig. 7a). As shown in Fig. 7b, serum AST and ALT levels were remarkably

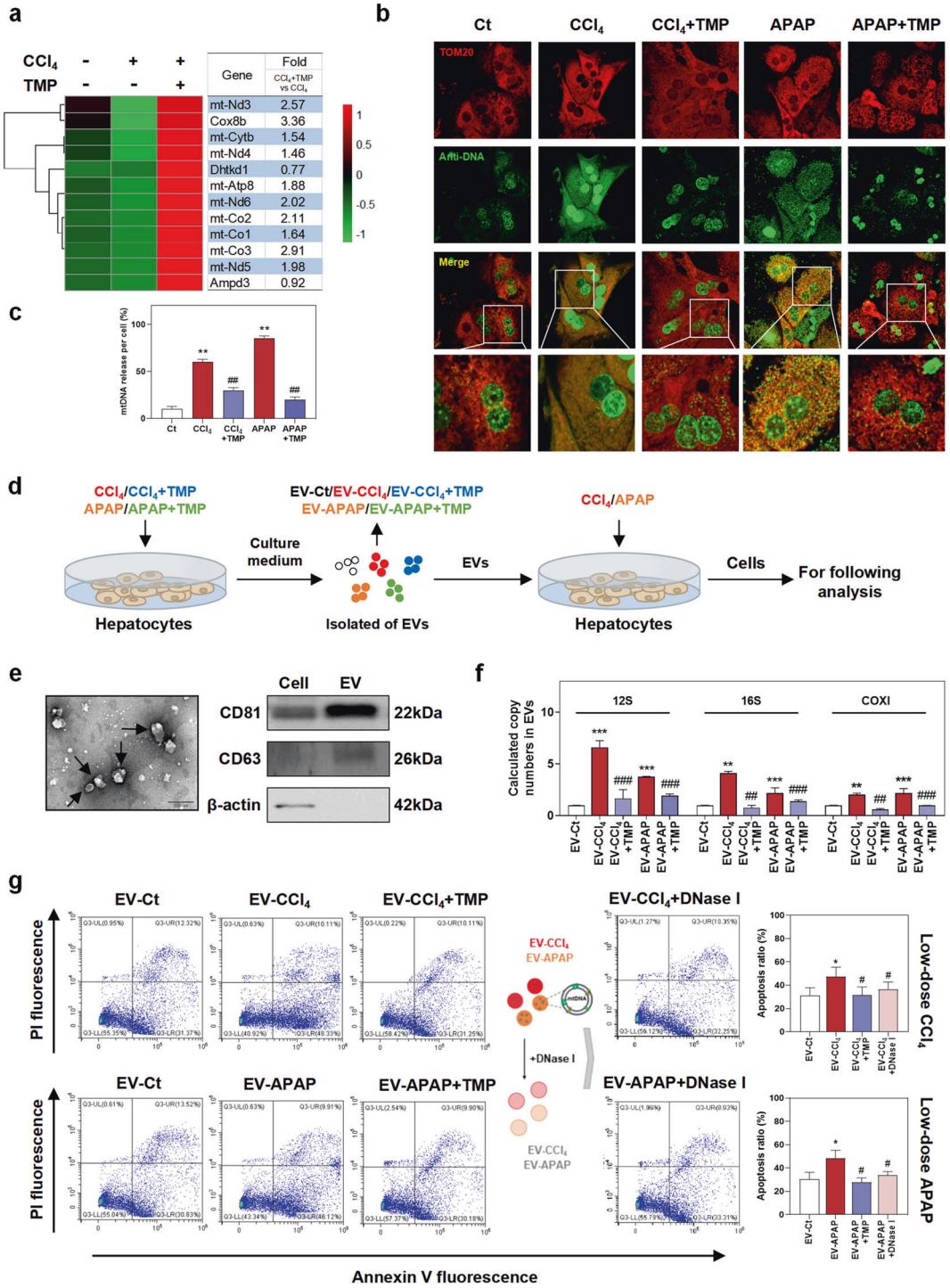

Fig. 4 TMP alleviates hepatocyte death by inhibiting mtDNA release in injured hepatocytes. Mice were treated as described in Fig. 1. **a** The relative expression levels of DEGs implicated in mtDNA synthesis were shown as a heatmap. Average log2 fold changes of CCl_4 + TMP vs CCl_4 groups were presented in the right panel. MPH were treated as described in Fig. 3. **b**, **c** Representative images and histograms of co-staining of TOM20 (red) and anti-DNA (green) in MPHs. mtDNA in mitochondria was characterized as localization (shown as yellow) and cytoplasmic free DNA outside nuclear and mitochondria area was shown as green dots. After pre-treated with 5 mM CCl_4 or 4 mM APAP for 1 h, MPHs were incubated with EVs from MPHs treated as described in Fig. 3 for 24 h. DNase I was used to deplete all mtDNA in EVs. **d** Experimental protocol. **e** TEM image for isolated EVs was shown in the left panel. Representative immunoblots against CD81, CD63, and β-ACTIN were shown in the right panel. **f** Copy numbers of 12S, 16S, and COXI were determined by qPCR and normalized with μL of EVs. **g** Experimental protocol and flow cytometry of AV-PI with histograms. Statistical significance: $^{*}P < 0.05$, $^{**}P < 0.01$, $^{***}P < 0.001$, compared with control group; $^{\#}P < 0.05$, $^{\#\#}P < 0.01$, $^{\#\#\#}P < 0.001$, compared with relative model group ($n = 3$).

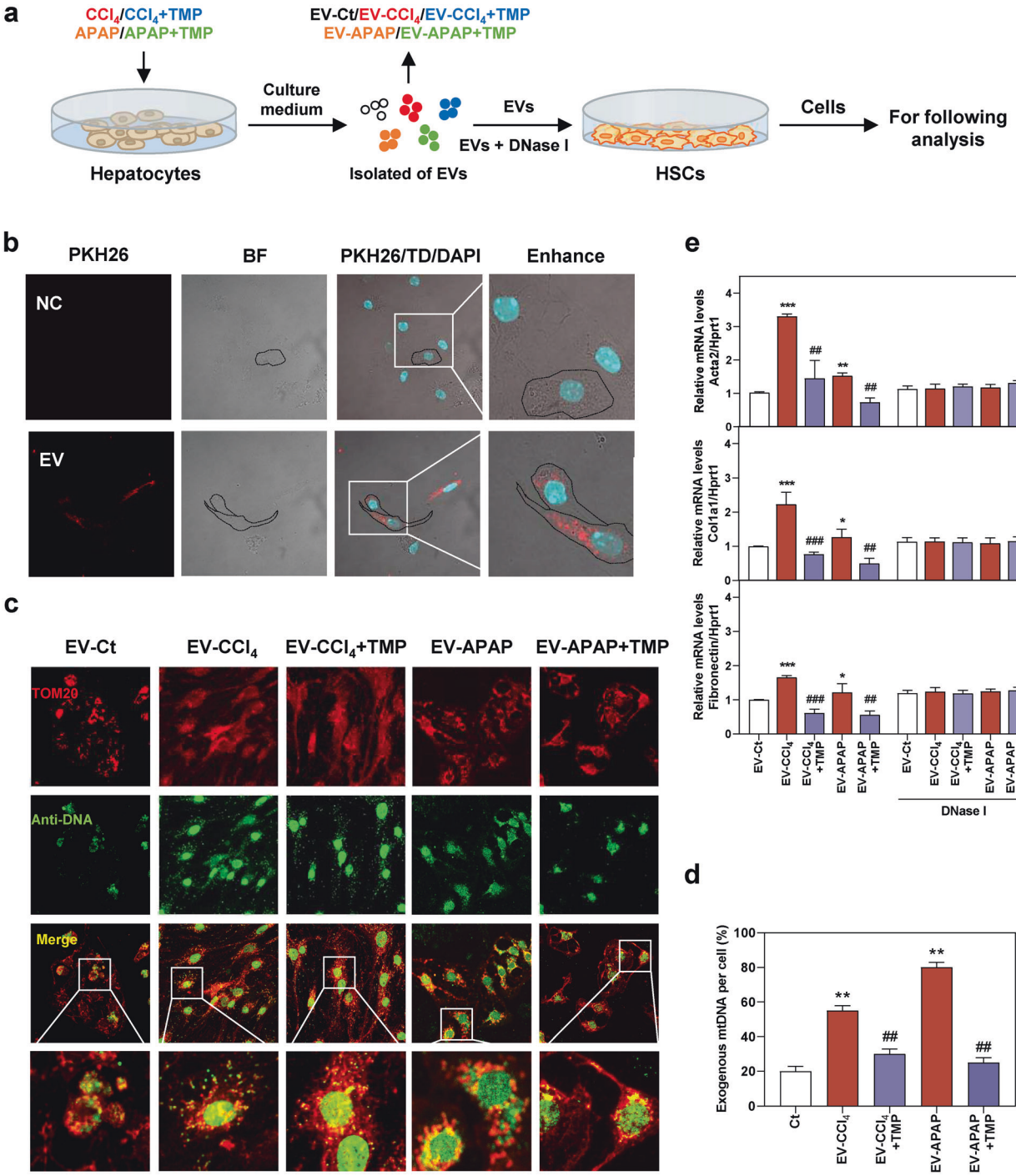

Fig. 5 TMP inhibits HSC activation by preventing mtDNA release in injured hepatocytes. Mouse primary HSCs were incubated with EVs from MPHs treated with CCl_4, CCl_4 + TMP, APAP and APAP + TMP for 48 h. **a** Experimental protocol. **b** Representative images of PKH26-labeled EVs taken up by primary mouse HSCs were shown. BF bright field. **c**, **d** Representative images and histograms of co-immunofluorescent staining of TOM20 and anti-DNA in HSCs. mtDNA in HSCs was characterized as colocalization of both TOM20 staining and anti-DNA signal (shown as yellow dots) and cytoplasmic free DNA outside nuclear and mitochondria area was shown as green dots. **e** Relative mRNA levels of *Acta2*, *Col1a1*, and *Fibronectin* in HSCs were determined by qPCR and normalized using *Hprt1* as an internal control. Statistical significance: $^{*}P < 0.05$, $^{**}P < 0.01$, $^{***}P < 0.001$, compared with control group; $^{\#\#}P < 0.01$, $^{\#\#\#}P < 0.001$, compared with relative model group ($n = 3$).

increased in the SEV-CCl_4 group and then significantly decreased in the SEV-CCl_4 + TMP group. In line with these findings, serum EVs derived from CCl_4-treated mice but not EVs from CCl_4 + TMP-treated mice triggered a certain degree of hepatocyte vacuolar damage and inflammation in the liver (Fig. 7c). Hepatic mRNA levels of *Gpx6*, *Gstt1*, *Gstm2*, *Gstt2*, and *Gpx3* were significantly decreased by SEV-CCl_4 injection. SEV-CCl_4 + TMP treatment, on the other hand, enhanced hepatic tolerance to oxidative stress (Fig. 7d and Supplementary Fig. S5a). The mtDNA levels in serum EVs were further determined in response to the transplantation of damage-related EVs. Interestingly, copy numbers of 12S, 16S, and COXI were significantly increased by SEV-CCl_4 for about 40, 16, and 10 folds, respectively. However, these mtDNA genes were only induced by SEV-CCl_4 + TMP injection for less than 7, 2, and 2 folds

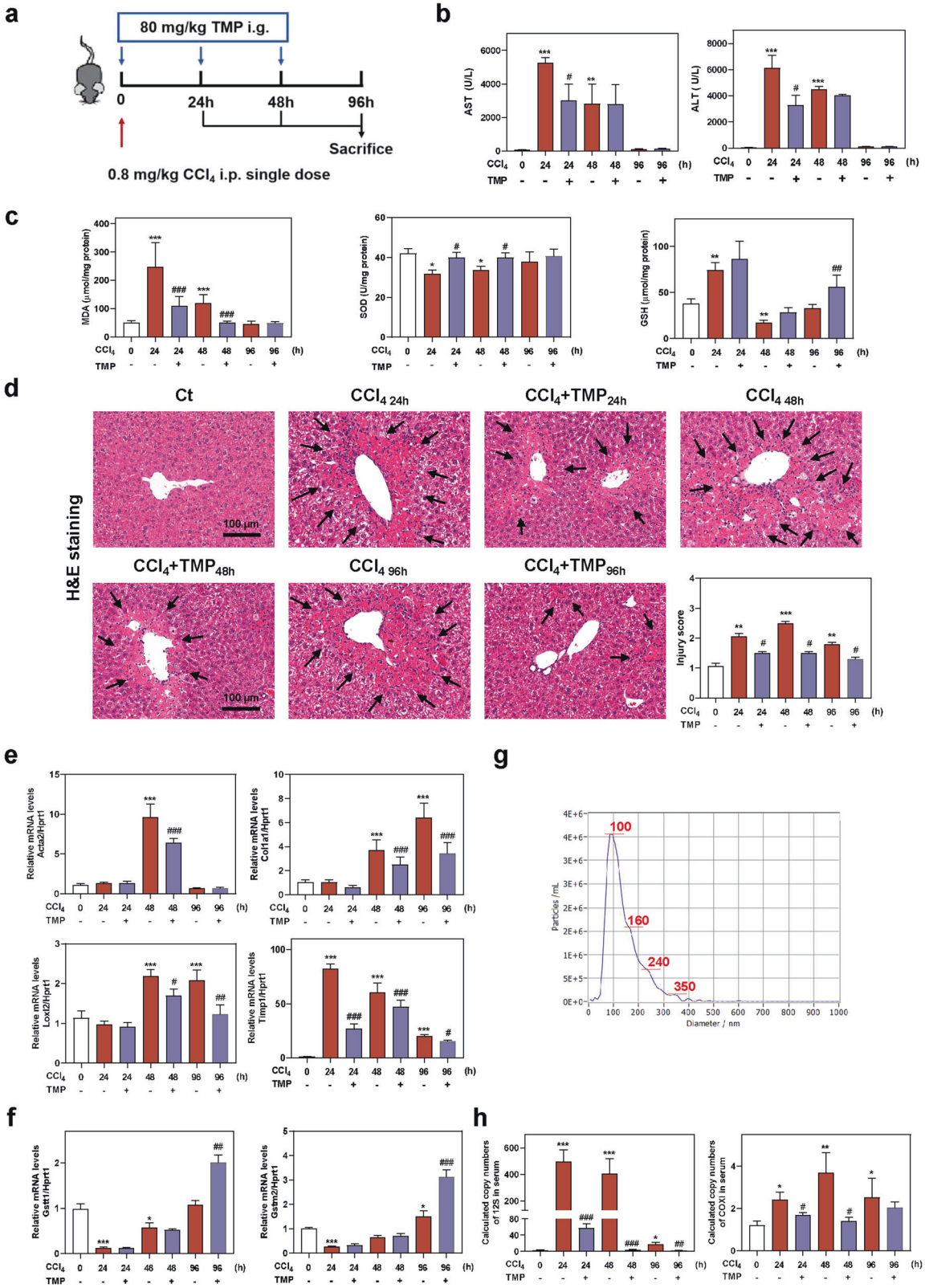

Fig. 6 TMP ameliorates CCl_4-induced acute liver injury and reduces mtDNA in serum. Mice were intraperitoneally injected with a single dose of CCl_4 (0.8 mg/kg) and treated with TMP (80 mg/kg) for 24, 48, and 96 h by gavage. **a** Experimental protocol. **b** AST and ALT levels in serum. **c** MDA, SOD, and GSH levels in livers. **d** Representative images of H&E staining. Scale bar = 100 μm. Relative mRNA levels of **e** *Acta2*, *Col1a1*, *Loxl2*, *Timp1*, **f** *Gstt1* and *Gstm2* were determined by qPCR and normalized using *Hprt1* as an internal control. **g** The mean size distribution and concentration ($3.9 \times e^9$) of particles in the NTA experiment. The red line represented the average of four readings. **h** Copy numbers of 12S and COXI in serum were determined by qPCR. Statistical significance: $^*P < 0.05$, $^{**}P < 0.01$, $^{***}P < 0.001$, compared with control group; $^{\#}P < 0.05$, $^{\#\#}P < 0.01$, $^{\#\#\#}P < 0.001$, compared with relative CCl_4 group ($n = 6$).

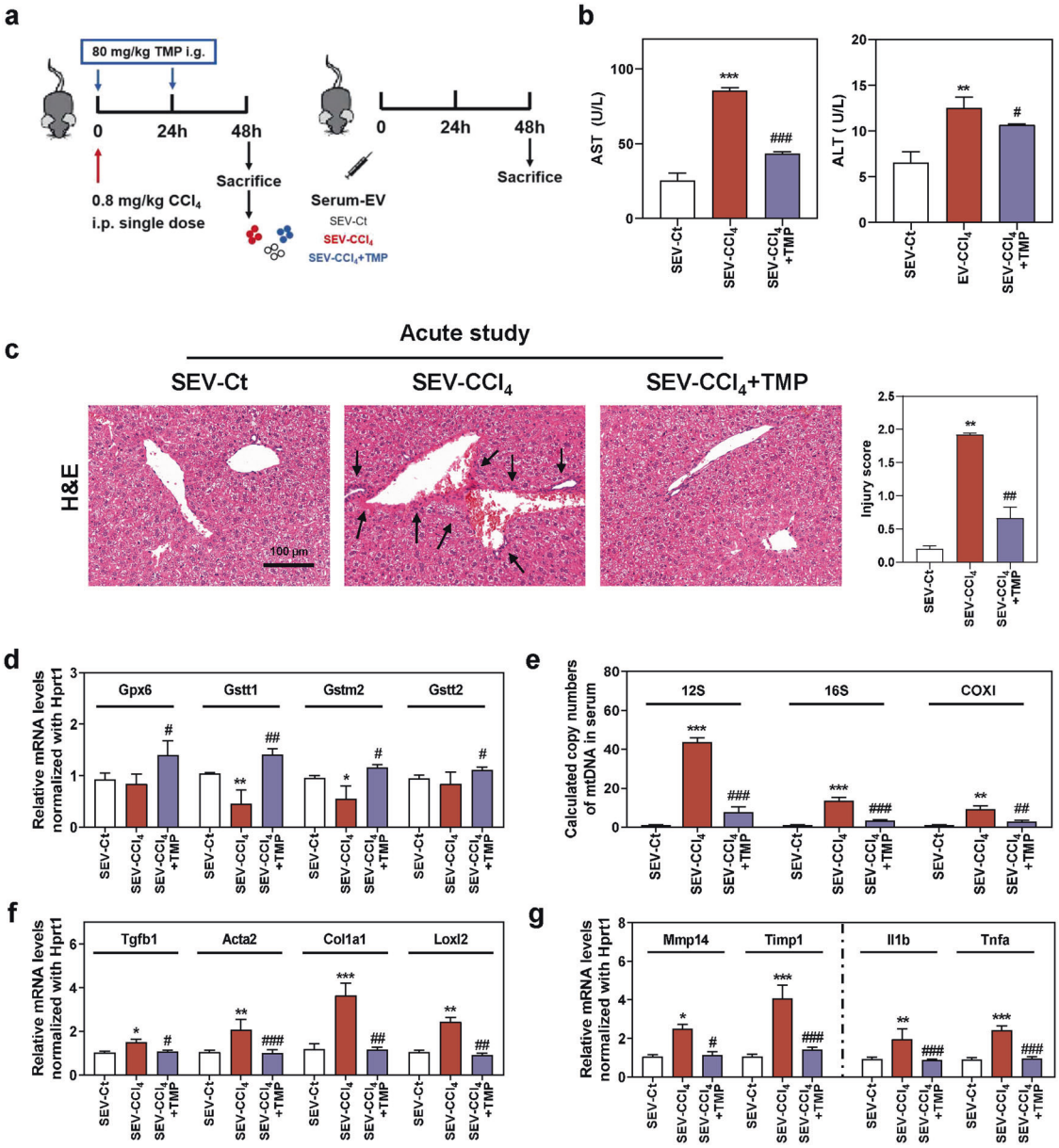

Fig. 7 TMP reduces CCl_4-mediated mtDNA enrichment in serum EVs and ameliorates mtDNA-induced hepatic injury. Mice were administered different serum EVs via tail vein injection for one time. **a** Experimental protocol. **b** AST and ALT levels in serum. **c** Representative images of H&E staining. Scale bar = 100 μm. Relative mRNA levels of **d** *Gpx6*, *Gstt1*, *Gstm2*, *Gstt2*, **f** *Tgfb1*, *Acta2*, *Col1a1*, *Loxl2*, **g** *Mmp14*, *Timp1*, *Il1b*, and *Tnfa* were determined by qPCR and normalized using *Hprt1* as an internal control. **e** Copy numbers of 12S, 16S, and COXI were determined by qPCR and normalized with μl of serum. Statistical significance: $^{*}P < 0.05$, $^{**}P < 0.01$, $^{***}P < 0.001$, compared with SEV-Ct; $^{\#}P < 0.05$, $^{\#\#}P < 0.01$, $^{\#\#\#}P < 0.001$, compared with SEV-CCl_4 group ($n = 6$).

when compared to the control group (Fig. 7e). Although substantial ECM accumulation was not observed in mice treated with SEV-CCl_4 (Fig. 7c), the hepatic mRNA levels of genes associated with collagen deposition, such as *Tgfb1*, *Acta2*, *Col1a1*, and *Loxl2* (Fig. 7f), and pro-inflammatory genes, such as *Il1b*, *Tnfa*, and *Il6* (Fig. 7g and Supplementary Fig. S5b) were significantly upregulated by the transplantation of SEV-CCl_4, when compared with SEV-Ct and SEV-CCl_4 + TMP group. Also, the balance of ECM degradation was interrupted in the SEV-CCl_4 group, as indicated by increased *Mmp14* mRNA level and even enhanced expression of its inhibitor *Timp1*, which was recovered by SEV-CCl_4 + TMP treatment (Fig. 7g). Collectively, mtDNA-containing EVs alone were sufficient to stimulate liver injury and fibrosis-related genes expression within 48 h, suggesting its pathogenic potential in the development of liver fibrosis, if continuously existing.

Serum EVs derived from CCl_4-treated mice, but not EVs derived from TMP-treated mice, promoted CCl_4-induced mild fibrosis

We further investigated whether mtDNA-containing EVs aggravated the fibrotic response in mild and chronic liver fibrosis and whether the hepatoprotective effects of TMP relied on the inhibition of mtDNA-containing EVs released from injured mice. After establishing mild liver fibrosis by 3-week administration of CCl_4, mice were then injected with SEV-Ct, SEV-CCl_4 and SEV-CCl_4 + TMP twice a week for 1 week as described in the Materials and Methods (Fig. 8a). As shown in Fig. 8b, although no significant change of serum AST between SEV-CCl_4 and SEV-CCl_4 + TMP groups was observed, the hepatoprotective activity of SEV-CCl_4 + TMP was corroborated by alleviated ALT level in serum. Liver histopathology analysis indicated that immune cell infiltration and collagen deposition were improved in mice treated with SEV-CCl_4

+ TMP when compared with those treated with SEV-CCl_4 (Fig. 8c). Multiple injections of mtDNA-enriched EVs derived from CCl_4 mice caused dramatic upregulation of pro-fibrogenic genes, including *Acta2*, *Col1a1*, *Loxl2* and *Timp1*, in recipient mice. On the other hand, SEV-CCl_4 + TMP significantly prevented CCl_4-induced mild liver fibrosis, as indicated by lower mRNA levels of fibrotic genes and a higher mRNA level of *Mmp14* compared to the SEV-CCl_4 group (Fig. 8d and Supplementary Fig. S6a). Furthermore, SEV-CCl_4 + TMP markedly decreased the protein expression of COL1A1 and α-SMA in livers compared with the SEV-CCl_4 group (Supplementary Fig. S6b). Interestingly, SEV-CCl_4 + TMP almost failed to impact mRNA levels of oxidative stress genes when compared to the SEV-CCl_4 group (Fig. 8e). These results might be due to the formation of a new dynamic balance between oxidation and reduction during the long-term CCl_4 challenge.

DISCUSSION

Liver fibrosis represents a dynamic wound healing process involving multi-cellular response and intercellular communication. Once damaged and/or even dead, hepatocytes rapidly exacerbate the release of multiple intracellular "danger signals" called DAMPs, which further trigger the inflammatory or innate immune response to participate in fibrogenesis [24]. HSCs are the major cellular source of hepatic ECM production and their transdifferentiation into aHSCs are decisive events in the entire process of liver fibrosis. Prior studies reported that hepatocyte-derived DAMPs contributed to the pathogenesis of liver fibrosis by activating HSCs, but underlying mechanisms were still obscure [25]. Hence, the identification of key mediators released from injured hepatocytes, particularly at very early stages, along with a better understanding of how they promote hepatocyte injury and HSC activation, are critical for discovering novel targets and therapies for the treatment of liver fibrosis. Recently, TMP was reported to alleviate liver injury via interrupting NLRP3 [26] and inhibit HSC-mediated vascular remodeling via interfering with pro-fibrogenic pathways [13]. In the current study, we demonstrated that TMP inhibited oxidative stress, improved mitochondrial function and ameliorated liver fibrosis by regulating intercellular communication of mtDNA between hepatocytes and HSCs (Fig. 8f).

Until now, there is no Food and Drug Administration-approved anti-fibrotic drug [27, 28]. Expanding knowledge regarding the protective effects of natural products isolated from herbs has encouraged researchers to explore a new direction for drug discovery against fibrotic liver diseases [29]. TMP, exhibiting a broad spectrum of pharmacological activities including liver protection, has been widely used for the treatment of diseases associated with oxidative stress and inflammatory injury. Recently, TMP has been reported to inhibit the production of pro-angiogenic cytokines and suppress the migration and adhesion of HSCs. Besides, it efficaciously improves liver fibrosis and angiogenesis through the activation of PPARγ and transrepression of HIF-1 [13]. Although the anti-fibrotic function of TMP is not systematically studied in vivo, independent reports have found evidence of suppressed HSC cycle and inhibited NLRP3 inflammasome in a fibrotic mouse model treated with TMP [30, 31]. In the present study, we systemically investigated the therapeutic effects and underlying mechanisms of TMP on the CCl_4-induced chronic liver fibrotic mouse model (Fig. 1). Our results suggest that TMP markedly prevents liver fibrogenesis by regulating the expression of genes implicated in collagen synthesis and degradation.

Emerging evidence uncovers the role of oxidative stress as a vital inducer of liver fibrosis [32]. ROS, which is generated by an imbalance in the energy produced and consumed, contributes to the activation of the antioxidant system and GSH depletion [19]. Previous work has demonstrated that TMP protected kidney cells from arsenic-induced apoptosis by suppressing intracellular ROS production, increasing GSH levels and maintaining mitochondrial membrane potential [33]. Here we also noted a significant increase of GSH and mRNA levels of *Gstt1*, *Gpx3*, and *Gstm2* in the presence of TMP in the liver (Fig. 2). These results suggested that TMP inhibited the overactivation of oxidative stress by upregulating the key enzymes and substrates for ROS scavenging during the continuous stimulation of CCl_4. Mitochondria are not only a rich source of ROS but also the primary target of oxidative stress. BAX and BAK form oligomers and result in MOMP during oxidative stress. Mitochondrial inner membrane (MIM) is extruded through expanding BAX pores [21]. Thereafter, the extruded MIM eventually permeabilizes (also known as MIMP) and leads to the cytosolic release of mtDNA. On the other hand, Kim et al. reported that mtDNA fragments were released through pores formed by the voltage-dependent anion channel (VDAC) oligomers in live cells [34]. Our results showed that TMP rapidly suppressed oxidative stress, restored mitochondrial membrane potential, and prevented hepatocyte injury impaired by toxic stimuli (Fig. 3). Meanwhile, TMP markedly upregulated the mRNA levels of major mtDNA genes and reduced the release of mtDNA from injured hepatocytes (Fig. 4). Our RNA-sequencing results further demonstrated that TMP significantly decreased hepatic mRNA levels of BAK and BAX and potentially inhibited mitochondrial outer membrane pores widening (data not shown). These findings have emphasized the protective effects of TMP on both structure and function of mitochondria. However, potential mechanisms involved in the recognition and secretion of mtDNA from injured hepatocytes and whether TMP restores the integrity of mitochondrial pores remain to be identified in future studies.

Emerging evidence indicates that mitochondrial damage appears to be a requisite step in intrinsic cell death pathways. Our results in Fig. 3 showed that TMP effectively restored hepatocyte function, prevented the production of ROS in or around mitochondria, leading to the increase of mitochondrial membrane potential. Here, we observed that mtDNA-containing EVs secreted by injured hepatocyte aggravated hepatocyte death (Fig. 4). Furthermore, we reported a novel mechanism by demonstrating the crosstalk between injured hepatocytes and HSCs via the transfer of mtDNA by EVs (Fig. 5). These effects of mtDNA-containing EVs on hepatocytes and HSCs were completely blocked after TMP interference or pre-incubation with DNase I. A growing number of studies provide general ideas of how liver cells-derived circulating EVs affect the progression of liver fibrosis. Recently, studies regarding the role of mitochondria-derived DAMPs in cell-to-cell communication have stepped into a new stage. After chronic CCl_4 plus alcohol exposure, aldehyde dehydrogenase 2 (Aldh2)-deficient hepatocytes exacerbated the release of harmful oxidized mtDNA-carrying EVs to neighboring hepatocytes, which activated oncogenic pathways and thus promoted fibrotic injury [35]. Another study also pointed out that thioacetamide promoted the release of mitochondrial DAMPs-enriched EVs from damaged hepatocytes into circulation, induced HSC activation and exaggerated fibrotic response in mice [7]. Together with our findings, we speculate that TMP may not only initially prevent mitochondrial oxidative stress and block continuous hepatocyte damage caused by mtDNA-containing EVs but also primarily decrease the delivery of mtDNA from hepatocytes into HSCs via EVs.

Researchers have already noticed the critical role of circulating mitochondrial DAMPs in promoting inflammatory response a decade ago [20]. In addition, high levels of hepatocyte-derived and mtDNA-enriched microparticles were detected in the liver and blood from fibrotic mice and patients, while scavenging circulating mtDNA might provide a therapeutic option for liver fibrosis and its complications [36, 37]. These findings highlight a promising correlation between injured hepatocyte-derived

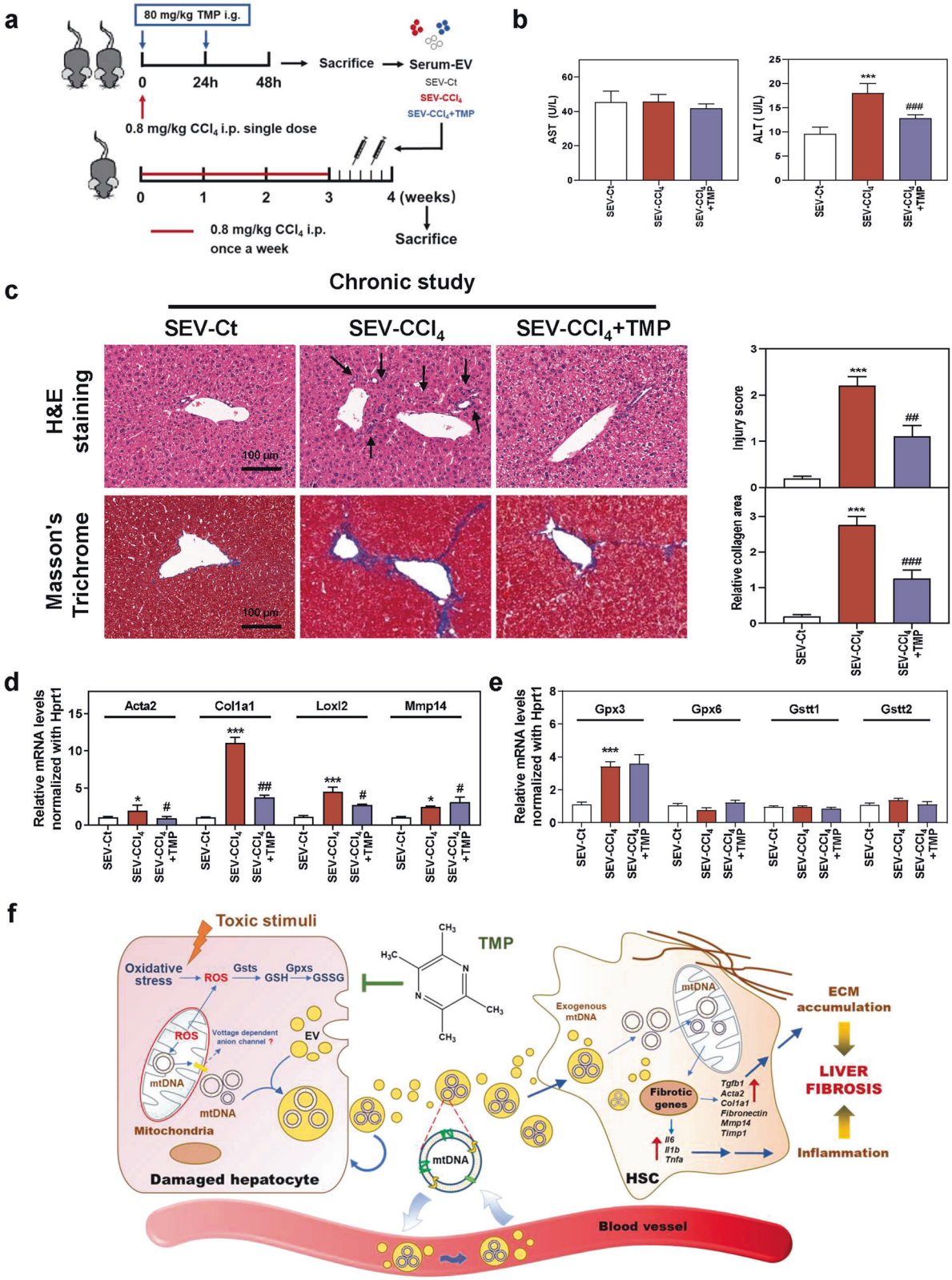

Fig. 8 Transplant of serum EVs derived from TMP-administered mice slows down the progression of chronic liver fibrosis. Mice were treated with CCl_4 or olive oil once a week for 3 weeks and then administered different serum EVs via tail vein injection two times. **a** Experimental protocol. **b** AST and ALT levels in serum. **c** Representative images of H&E and Masson's Trichrome staining. Scale bar = 100 μm. Relative mRNA levels of **d** *Acta2*, *Col1a1*, *Loxl2*, *Mmp14*, **e** *Gpx3*, *Gpx6*, *Gstt1*, and *Gstt2* were determined by qPCR and normalized using *Hprt1* as an internal control. **f** Schematic diagram of the proposed mechanism underlying the hepatoprotective effects of TMP on oxidative stress in hepatocytes, HSC activation and fibrotic response during liver fibrosis. Statistical significance: $^{*}P < 0.05$, $^{***}P < 0.001$, compared with SEV-Ct; $^{\#}P < 0.05$, $^{\#\#}P < 0.01$, $^{\#\#\#}P < 0.001$, compared with SEV-CCl_4 group ($n = 6$).

mtDNA and liver fibrosis progression. Although the role of mtDNA released from damaged cells in initiating or amplifying inflammatory response is gradually recognized, a recent study reported that mitochondrial DAMPs, mainly mtDNA, leaked from injured hepatocytes were directly responsible for triggering HSC activation and fibrotic response independently of their pro-inflammatory effects [7]. These findings were supported by our results about the effects of hepatocyte-releasing EV-CCl_4 and EV-CCl_4 + TMP on HSC activation. The expression of fibrosis-related genes was significantly increased after EV-CCl_4 treatment but decreased by EVs derived from MPHs in the presence of TMP (Fig. 5). However, these EVs mostly failed to impact the expression of inflammatory factors (data not shown). On the other hand, a most recent study reported that the mitochondrial respiration and copy number of mtDNA were significantly higher in aHSCs than qHSCs, potentially because aHSCs exhibited a higher basal respiration rate to meet their high energy demand [38]. Consistently, we demonstrated that TMP markedly prevented the transfer of exogenous mtDNA from hepatocytes to HSC and decreased mtDNA copy numbers in the cytoplasm (Fig. 5). In addition, TMP alone and combined with paeonol promoted apoptosis and inhibited the mitochondrial activity of aHSC, suggesting that TMP might directly regulate the mitochondrial function of HSCs and thus hamper their activation [39].

Another interesting finding from this study was that serum mtDNA levels were rapidly increased at 24 h and decreased 96 h after CCl_4 treatment, which was prior to the upregulation of fibrosis-related genes and pathological injury in livers (Fig. 6), suggesting that damage-related mtDNA is the cause but not the consequence of liver fibrogenic response. Consistently, after one-time injection of serum EVs derived from CCl_4-treated mice, mtDNA level was dramatically upregulated in serum and was further accompanied with mild liver injury and rapid increase of mRNA levels of fibrotic genes in the liver (Fig. 7). Our results highlighted that protective effects of TMP against liver fibrosis were largely due to the inhibition of oxidative stress-mediated mtDNA leakage in hepatocytes and mtDNA-enriched EVs-mediated HSC activation (Fig. 8). These data further suggested that mtDNA-enriched EVs in circulation represent a potential diagnostic biomarker as well as a potential therapeutic target for liver fibrosis.

CONCLUSION

Taken together, our results indicate that TMP ameliorates hepatic oxidative stress and improves liver fibrosis in both CCl_4-induced acute and chronic liver injury mouse models. TMP also recovers toxic chemicals-impaired mitochondrial membrane potential of hepatocytes, prevents the release of mtDNA from injured hepatocytes and thus mitigates hepatocyte death and HSCs activation stimulated by mtDNA-enriched EVs (Fig. 8f). Our study not only provides new insights into the complex mechanisms by which TMP protects against liver fibrosis but also offers a conceptual framework for the future discovery of TMP-based or other innovative therapeutic agents for the treatment of liver fibrosis by targeting intercellular communication.

ACKNOWLEDGEMENTS

This work was supported by the Beijing Municipal Science & Technology Commission (Grant No. 7212174 to XL); National Natural Science Foundation of China (Grant No. 82004045 to XL); Beijing Nova Program of Science & Technology (Grant No. Z191100001119088 to XL; Grant No. Z201100006820025 to RL); and the Young Talents Promotion Project of China Association of Traditional Chinese Medicine (Grant No. 2020-QNRC2-01 to XL); Innovation Team and Talents Cultivation Program of National Administration of Traditional Chinese Medicine (Grant No. ZYYCXTD-C-202006 to XL).

AUTHOR CONTRIBUTIONS

XL and RPL conceived the original idea and supervised the study. XL, YJL, and RPL prepared the manuscript and figures. YJL, MND, QZ, JZW, XYX, YQG, BNM, YJC, Shuo Li, Sheng Lin, and LYZ conducted all the experiments. YJL, MND, JZW, and XYX performed data analysis. All authors have approved the final manuscript.

ADDITIONAL INFORMATION

Supplementary information The online version contains supplementary material available at https://doi.org/10.1038/s41401-021-00843-w.

Competing interests: The authors declare no competing interests.

REFERENCES

1. Li Y, Liu R, Wu J, Li X. Self-eating: friend or foe? The emerging role of autophagy in fibrotic diseases. Theranostics. 2020;10:7993–8017.
2. Hirsova P, Ibrahim SH, Verma VK, Morton LA, Shah VH, LaRusso NF, et al. Extracellular vesicles in liver pathobiology: small particles with big impact. Hepatology. 2016;64:2219–33.
3. Liu R, Li X, Zhu W, Wang Y, Zhao D, Wang X, et al. Cholangiocyte-derived exosomal long noncoding RNA H19 promotes hepatic stellate cell activation and cholestatic liver fibrosis. Hepatology. 2019;70:1317–35.
4. Dasgupta D, Nakao Y, Mauer AS, Thompson JM, Sehrawat TS, Liao CY, et al. IRE1A stimulates hepatocyte-derived extracellular vesicles that promote inflammation in mice with steatohepatitis. Gastroenterology. 2020;159:1487–503.e17.
5. Jiang F, Chen Q, Wang W, Ling Y, Yan Y, Xia P. Hepatocyte-derived extracellular vesicles promote endothelial inflammation and atherogenesis via microRNA-1. J Hepatol. 2020;72:156–66.
6. Povero D, Panera N, Eguchi A, Johnson CD, Papouchado BG, de Araujo Horcel L, et al. Lipid-induced hepatocyte-derived extracellular vesicles regulate hepatic stellate cell via microRNAs targeting PPAR-γ. Cell Mol Gastroenterol Hepatol. 2015;1:646–63.e4.
7. An P, Wei LL, Zhao S, Sverdlov DY, Vaid KA, Miyamoto M, et al. Hepatocyte mitochondria-derived danger signals directly activate hepatic stellate cells and drive progression of liver fibrosis. Nat Commun. 2020;11:2362.
8. Chen L, Chen R, Kemper S, Brigstock DR. Pathways of production and delivery of hepatocyte exosomes. J Cell Commun Signal. 2018;12:343–57.
9. Li X, Chen R, Kemper S, Brigstock DR. Extracellular vesicles from hepatocytes are therapeutic for toxin-mediated fibrosis and gene expression in the liver. Front Cell Dev Biol. 2019;7:368.
10. Dansako H, Ueda Y, Satoh S, Kato N. Extracellular vesicles activate ATM-Chk2 signaling pathway through the intercellular transfer of mitochondrial DNA in HBV-infected human hepatocytes. FASEB J. 2021;35:e21680.
11. Zhao S, Zhang Z, Yao Z, Shao J, Chen A, Zhang F, et al. Tetramethylpyrazine attenuates sinusoidal angiogenesis via inhibition of hedgehog signaling in liver fibrosis. IUBMB Life. 2017;69:115–27.
12. Gao B, Lin X, Jing H, Fan J, Ji C, Jie Q, et al. Local delivery of tetramethylpyrazine eliminates the senescent phenotype of bone marrow mesenchymal stromal cells and creates an anti-inflammatory and angiogenic environment in aging mice. Aging Cell. 2018;17:e12741.
13. Zhang F, Lu S, He J, Jin H, Wang F, Wu L, et al. Ligand activation of PPARγ by ligustrazine suppresses pericyte functions of hepatic stellate cells via SMRT-mediated transrepression of HIF-1α. Theranostics. 2018;8:610–26.
14. Cai Y, Xu B, Zhou F, Wu J, Li S, Zheng Q, et al. Si-Ni-San ameliorates chronic colitis by modulating type I interferons-mediated inflammation. Phytomedicine. 2021;84:153495.
15. Li X, Liu R, Yang J, Sun L, Zhang L, Jiang Z, et al. The role of long noncoding RNA H19 in gender disparity of cholestatic liver injury in multidrug resistance 2 gene knockout mice. Hepatology. 2017;66:869–84.
16. Mailloux RJ, Treberg JR. Protein S-glutathionlyation links energy metabolism to redox signaling in mitochondria. Redox Biol. 2016;8:110–8.
17. Li X, Liu R, Wang Y, Zhu W, Zhao D, Wang X, et al. Cholangiocyte-derived exosomal lncRNA H19 promotes macrophage activation and hepatic inflammation under cholestatic conditions. Cells. 2020;9:190.
18. Bock FJ, Tait SWG. Mitochondria as multifaceted regulators of cell death. Nat Rev Mol Cell Biol. 2020;21:85–100.
19. Ruart M, Chavarria L, Campreciós G, Suárez-Herrera N, Montironi C, Guixé-Muntet S, et al. Impaired endothelial autophagy promotes liver fibrosis by aggravating the oxidative stress response during acute liver injury. J Hepatol. 2019;70:458–69.
20. Zhang Q, Raoof M, Chen Y, Sumi Y, Sursal T, Junger W, et al. Circulating mitochondrial DAMPs cause inflammatory responses to injury. Nature. 2010;464:104–7.
21. Riley JS, Quarato G, Cloix C, Lopez J, O'Prey J, Pearson M, et al. Mitochondrial inner membrane permeabilisation enables mtDNA release during apoptosis. EMBO J. 2018;37:37.

22. Dong J, Viswanathan S, Adami E, Singh BK, Chothani SP, Ng B, et al. Hepatocyte-specific IL11 cis-signaling drives lipotoxicity and underlies the transition from NAFLD to NASH. Nat Commun. 2021;12:66.
23. Saikia M, Nath R, Devi D. Genetic diversity and phylogeny analysis of *Antheraea assamensis* Helfer (Lepidoptera: Saturniidae) based on mitochondrial DNA sequences. J Genet. 2019;98:98.
24. Mooring M, Fowl BH, Lum S, Liu Y, Yao K, Softic S, et al. Hepatocyte stress increases expression of yes-associated protein and transcriptional coactivator with PDZ-binding motif in hepatocytes to promote parenchymal inflammation and fibrosis. Hepatology. 2020;71:1813–30.
25. Ge X, Arriazu E, Magdaleno F, Antoine DJ, Dela Cruz R, Theise N, et al. High mobility group box-1 drives fibrosis progression signaling via the receptor for advanced glycation end products in mice. Hepatology. 2018;68:2380–404.
26. Zhang F, Jin H, Wu L, Shao J, Wu X, Lu Y, et al. Ligustrazine disrupts lipopolysaccharide-activated NLRP3 inflammasome pathway associated with inhibition of Toll-like receptor 4 in hepatocytes. Biomed Pharmacother. 2016;78:204–9.
27. Roehlen N, Crouchet E, Baumert TF. Liver fibrosis: mechanistic concepts and therapeutic perspectives. Cells. 2020;9:9.
28. Konerman MA, Jones JC, Harrison SA. Pharmacotherapy for NASH: current and emerging. J Hepatol. 2018;68:362–75.
29. Zhang Y, Jiang M, Cui BW, Jin CH, Wu YL, Shang Y, et al. P2X7 receptor-targeted regulation by tetrahydroxystilbene glucoside in alcoholic hepatosteatosis: a new strategy towards macrophage-hepatocyte crosstalk. Br J Pharmacol. 2020;177:2793–811.
30. Hu J, Cao G, Wu X, Cai H, Cai B. Tetramethylpyrazine inhibits activation of hepatic stellate cells through hedgehog signaling pathways in vitro. Biomed Res Int. 2015;2015:603067.
31. Ma X, Ruan Q, Ji X, Yang J, Peng H. Ligustrazine alleviates cyclophosphamide-induced hepatotoxicity via the inhibition of Txnip/Trx/NF-kappaB pathway. Life Sci. 2021;274:119331.
32. Luangmonkong T, Suriguga S, Mutsaers H, Groothuis G, Olinga P, Boersema M. Targeting oxidative stress for the treatment of liver fibrosis. Rev Physiol Biochem Pharmacol. 2018;175:71–102.
33. Gong X, Ivanov VN, Davidson MM, Hei TK. Tetramethylpyrazine (TMP) protects against sodium arsenite-induced nephrotoxicity by suppressing ROS production, mitochondrial dysfunction, pro-inflammatory signaling pathways and programed cell death. Arch Toxicol. 2015;89:1057–70.
34. Kim J, Gupta R, Blanco LP, Yang S, Shteinfer-Kuzmine A, Wang K, et al. VDAC oligomers form mitochondrial pores to release mtDNA fragments and promote lupus-like disease. Science. 2019;366:1531–6.
35. Seo W, Gao Y, He Y, Sun J, Xu H, Feng D, et al. ALDH2 deficiency promotes alcohol-associated liver cancer by activating oncogenic pathways via oxidized DNA-enriched extracellular vesicles. J Hepatol. 2019;71:1000–11.
36. Garcia-Martinez I, Santoro N, Chen Y, Hoque R, Ouyang X, Caprio S, et al. Hepatocyte mitochondrial DNA drives nonalcoholic steatohepatitis by activation of TLR9. J Clin Invest. 2016;126:859–64.
37. Aswani A, Manson J, Itagaki K, Chiazza F, Collino M, Wupeng WL, et al. Scavenging circulating mitochondrial DNA as a potential therapeutic option for multiple organ dysfunction in trauma hemorrhage. Front Immunol. 2018;9:891.
38. Bae M, Lee Y, Park YK, Shin DG, Joshi P, Hong SH, et al. Astaxanthin attenuates the increase in mitochondrial respiration during the activation of hepatic stellate cells. J Nutr Biochem. 2019;71:82–89.
39. Kong D, Chen L, Huang W, Zhang Z, Wang L, Zhang F, et al. Combined therapy with ligustrazine and paeonol mitigates hepatic fibrosis through destroying mitochondrial integrity of stellate cell. Am J Transl Res. 2020;12:1255–66.